PHYSICAL REVIEW E **94**, 060201(R) (2016)

Oscillation structure of localized perturbations in modulationally unstable media

Gino Biondini,[1,2] Sitai Li,[2] and Dionyssios Mantzavinos[2]
[1]*Department of Physics, State University of New York at Buffalo, Buffalo, New York 14260, USA*
[2]*Department of Mathematics, State University of New York at Buffalo, Buffalo, New York 14260, USA*
(Received 16 May 2016; published 23 December 2016)

We characterize the properties of the asymptotic stage of modulational instability arising from localized perturbations of a constant background, including the number and location of the individual peaks in the oscillation region. We show that, for long times, the solution tends to an ensemble of classical (i.e., sech-shaped) solitons of the focusing nonlinear Schrödinger equation (as opposed to the various breatherlike solutions of the same equation with a nonzero background). We also confirm the robustness of the theoretical results by comparing the analytical predictions with careful numerical simulations with a variety of initial conditions, which confirm that the evolution of modulationally unstable media in the presence of localized initial perturbations is indeed described by the same asymptotic state.

DOI: 10.1103/PhysRevE.94.060201

Introduction. The dynamics of media subject to modulational instability (MI) [1] has received renewed attention in recent years, thanks in part to its connections to the phenomena of rogue waves and integrable turbulence [2–6] and in part to a number of theoretical and experimental advances [7–14]. The prototypical model for the study of such phenomena is the focusing nonlinear Schrödinger (NLS) equation,

$$iq_t + q_{xx} + 2\big(|q|^2 - q_o^2\big)q = 0, \tag{1}$$

where subscripts x and t denote partial derivatives and $q_o > 0$ is the background amplitude. In particular, Eq. (1) describes the envelope dynamics in deep water waves, optical fibers, and attracting Bose-Einstein condensates [15–17]. [The term $2q_o^2 q$ in Eq. (1), which can be removed by the trivial gauge transformation $q(x,t) \mapsto q(x,t)e^{2iq_o^2 t}$, was added so that the boundary conditions are independent of time.]

From an applicative point of view, MI has many applications in optics, e.g., in the generation of supercontinuum light sources [18–20]. Recently, MI has also been applied in fiber optics as a novel sensing mechanism [21–24].

To study MI, one must look at the evolution of perturbations to the constant solution $q_{\rm cw}(x,t) = q_o$ of Eq. (1). The linear stage of MI, which is easily studied by linearizing Eq. (1) around the constant background solution $q_{\rm cw}$, exhibits exponential growth of long wavelength perturbations. The nonlinear stage of MI, however, which is reached once the perturbations have become comparable with the background, is much more complex, and has been the subject of intense study over the years, either with periodic boundary conditions (BCs) or with constant fields at infinity, i.e., with the nonzero boundary conditions (NZBCs) $\lim_{x\to\pm\infty} q(x,t) = q_o$.

Importantly, the nonlinear dynamics produced by MI is highly dependent on the nature of the spatial domain as well as the specific BC considered. In particular, for finite domains with periodic BCs, the solutions of Eq. (1) exhibit recurrence of initial conditions (ICs) [25,26], a phenomenon observed in water waves [27,28] as well as optics [29–32]. The same setting also displays sensitive dependence on ICs and numerically induced chaos [33,34]. Such chaotic phenomena, experimentally demonstrated in Ref. [35], are attributed to the presence of homoclinic solutions of Eq. (1) with periodic BCs [36,37].

The dynamics produced by MI on infinite spatial domains is very different, however. In Ref. [12] we studied the nonlinear stage of MI for localized perturbations of the background using the inverse scattering transform for the focusing NLS equation with NZBCs [11]. We showed that MI is mediated by the continuous spectrum of the scattering problem associated with Eq. (1), whose growing solutions are the precise nonlinear analog of the unstable Fourier modes. In Refs. [13,14] we then showed that the long-time behavior of a large class of finite-energy perturbations of the constant background reaches the same asymptotic state. We emphasize that the presence of this asymptotic state of MI depends crucially on the BCs. In practice, the difference between a finite spatial domain with periodic BCs and an infinite domain with NZBCs is realized by seeding the IC with periodic perturbations as opposed to spatially localized ones.

The purpose of this Rapid Communication is twofold. First, building on Refs. [13,14], we characterize in detail the properties of the asymptotic state, which reveals a number of interesting phenomena. In particular, we show that, for long times, the solution tends to an ensemble of classical (i.e., sech-shaped) solitons of the NLS equation (as opposed to the various breatherlike solutions of the same equation with NZBCs). Second, we considerably strengthen the analytical results by comparing them with careful numerical simulations of Eq. (1) with a variety of ICs, which demonstrate the robustness of the theoretical predictions and confirm that indeed the asymptotic state describes the evolution of a large number of perturbations of the constant background.

Asymptotic state of MI. Recall [13,14] that, for a broad class of localized initial perturbations of the constant background, the solution has the asymptotic behavior $q(x,t) = q_{\rm asymp}(x,t) + O(1/\sqrt{t})$ as $t \to \infty$ with the xt plane divided into three regions: (i) two plane-wave regions, $x < -\xi_* t$ and $x > \xi_* t$ with $\xi_* = 4\sqrt{2}q_o$ in which $|q_{\rm asymp}(x,t)| = q_o$ (i.e., the solution has the same amplitude as the undisturbed background); (ii) a modulated elliptic wave region $-\xi_* t < x < \xi_* t$ in which the solution is expressed by a slow modulation of

the elliptic solutions of Eq. (1), namely,

$$|q_{\rm asymp}(x,t)|^2 = (q_o+\alpha_{\rm im})^2 - 4q_o\alpha_{\rm im}\,{\rm sn}^2[2C(x-2\alpha_{\rm re}t-X_o)|m], \quad (2)$$

where sn(·) is one of the Jacobian elliptic functions [38], $m\in[0,1]$ is the elliptic parameter, $C=\sqrt{q_o\alpha_{\rm im}/m}$, and the offset X_o depends on the IC $q(x,0)$ via the reflection coefficient [14]. When $\alpha_{\rm re}$ and $\alpha_{\rm im}$ are independent of x and t, Eq. (2) is an exact traveling wave solution of Eq. (1) with m given by Eq. (3c) below [39]. In our case, however, $\alpha_{\rm re}$, $\alpha_{\rm im}$, and m are slowly varying functions of x and t which are given by the following system of modulation equations [14,39,40]:

$$\frac{x}{2t} = 2\alpha_{\rm re} + \frac{q_o^2-\alpha_{\rm im}^2}{\alpha_{\rm re}}, \quad (3a)$$

$$m = \frac{4q_o\alpha_{\rm im}}{\alpha_{\rm re}^2+(q_o+\alpha_{\rm im})^2}, \quad (3b)$$

$$\left[\alpha_{\rm re}^2+(q_o-\alpha_{\rm im})^2\right]K(m) = \left(\alpha_{\rm re}^2-\alpha_{\rm im}^2+q_o^2\right)E(m), \quad (3c)$$

where $K(m)$ and $E(m)$ are the complete elliptic integrals of the first and second kinds, respectively. Importantly, these equations are universal, i.e., independent of the ICs [13,14].

We next use Eq. (3) to characterize the structure of the modulated elliptic wave region. For brevity we limit ourselves to considering the range of $x\geqslant 0$. (To obtain the corresponding results for the range of $x<0$, one can simply take the opposite of $\alpha_{\rm re}$ in the discussion below.) It is easy to show that in this case $\alpha_{\rm re}$ is also positive [14]. It is also convenient to introduce the similarity variable $\xi=x/t$.

A key step in order to characterize the properties of the modulated elliptic solution (2) is to express all quantities in Eq. (3) as functions of m. Doing so allows one to obtain ξ, $\alpha_{\rm re}$, and $\alpha_{\rm im}$ explicitly, thus eliminating the need to solve a nonlinear system of equations. Explicitly, Eq. (3) yields

$$\alpha_{\rm re}(m) = \frac{2q_o\sqrt{1-m}}{m}\sqrt{1-(1-m)\frac{K^2(m)}{E^2(m)}}, \quad (4a)$$

$$\alpha_{\rm im}(m) = \frac{q_o}{m}\left[2-m-2(1-m)\frac{K(m)}{E(m)}\right], \quad (4b)$$

with corresponding expressions for $\xi(m)$ and $C(m)$ (see the Appendix). Inserting these expressions in Eq. (2) and letting $x=\xi(m)t$ one can now compute $q_{\rm asymp}(x,t)$ explicitly as a function of m and t.

Equation (4) enables us to obtain a number of important properties of the asymptotic state. Recall that the limiting case $m\to 1$ of the elliptic solution (2) yields the sech-shaped solitons of the focusing NLS equation with zero background, whereas the limit $m\to 0$ yields the background solution. Note that $\xi(m)$ is a decreasing function of m as shown in Fig. 1(left) with $\xi(0)=\xi_*$ and $\xi(1)=0$. The behavior of $q_{\rm asymp}(x,t)$ as a function of x and t with $X_o=0$ also is shown in Fig. 2.

A signature of the nonlinear stage of MI is the local behavior of the solutions in the modulated elliptic wave region, which we turn to next. For simplicity, we consider the prototypical case of $X_o=0$. We show below, however, that the results agree very well with direct numerical simulations of Eq. (1) with a variety of ICs.

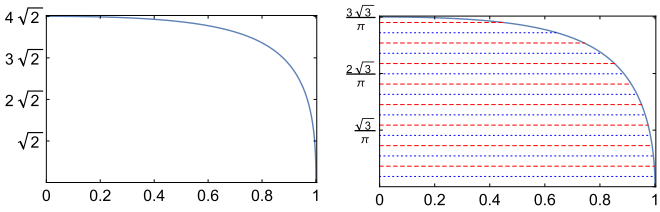

FIG. 1. The quantities $\xi(m)$ (left panel) and $f(m)$ (right panel) as functions of m for $q_o=1$. The red dashed lines identify the location of the peaks of $|q_{\rm asymp}|$ at $t=5$, and the dotted blue lines indicate the location of the troughs.

Let us denote by x_n the nth peak of $|q_{\rm asymp}(x,t)|$ as a function of t, counting from $x=0$. Notice that the origin $x=0$ is always a peak when $X_o=0$ as can be seen from Eq. (2). (Note however that there exist ICs for which a trough is present at $x=0$ instead of a peak. This is due to the fact that, for such ICs, the value of X_o at $m=1$ is not negligible.) Since $\alpha_{\rm im}>0$, Eq. (2) implies that such peaks are located along the zeros of sn. Since ${\rm sn}(0|m)=0$ and ${\rm sn}^2(\Theta|m)={\rm sn}^2(\Theta+2nK(m)|m)$ for $n\in\mathbb{Z}$, we have that the locations of the peaks are given by

$$x_n(t) = 2\alpha_{\rm re}(m)t + nK(m)/C(m). \quad (5)$$

Recall, however, that $x=\xi t$ is already determined as a function of m via Eq. (4) and Eq. (3a). Thus, Eq. (5) is actually a constraint on m, and the peak locations are given precisely by those values $m=m_n(t)$ which satisfy it. In other words, the parameter m in Eq. (5) is also time dependent. We rewrite Eq. (5) as

$$f(m) = n/t, \qquad n\in\mathbb{Z}, \quad (6)$$

where $f(m)$ is explicitly given in terms of m by

$$f(m) = \frac{C(m)}{K(m)}[\xi(m)-2\alpha_{\rm re}(m)]. \quad (7)$$

As shown in Fig. 1(right), $f(m)$ is also decreasing with m with $f(0)=3\sqrt{3}\,q_o/\pi$ and $f(1)=0$. [Equation (6) is reminiscent of the constraint that yields the allowed energy levels of a quantum-mechanical particle in a one-dimensional potential well. In this analogy, the parameter t in Eq. (6) is the analog of

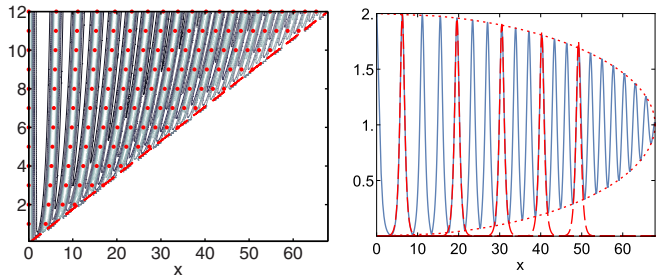

FIG. 2. Left panel: Contour plot of the asymptotic solution $|q_{\rm asymp}(x,t)|$ (2) on the xt plane for $q_o=1$ with the peak locations $x_n(t)$ (10) (red dots) and the boundary of the modulated region (dashed red line). Right panel: The asymptotic solution $|q_{\rm asymp}(x,t)|$ (2) with $q_o=1$ at $t=12$ as a function of x, together with five independent sech-like solutions $q_n(x,t)$ (12) (dashed red curves) and predicted envelope (dotted red curve).

the depth of the potential well, and a new eigenvalue appears whenever t increases by $3\sqrt{3}q_o/\pi$.]

Equation (6) can be solved numerically to obtain the values of $m_n(t)$ corresponding to the peaks. Such values can then be inserted in Eq. (5) to obtain the peak locations $x_n(t)$. As we show below, the resulting locations agree very well with the results of numerical simulations of Eq. (1) with a variety of ICs, confirming the universal nature of the asymptotic stage of MI. The location of the minima of $|q_{\text{asymp}}|$ can be obtained in a similar way.

As can be seen in Fig. 2, the number of oscillations increases with time. (This is confirmed by numerical results as discussed later.) Indeed, this is a direct consequence of Eq. (6). Denoting by $n_{\text{peak}}(t)$ the number of peaks for $x \in (0,4\sqrt{2q_o t})$ and recalling the behavior of $f(m)$ as a function of m, we immediately have

$$n_{\text{peak}}(t) = \lfloor (3\sqrt{3}/\pi) q_o^2 t \rfloor, \tag{8}$$

where $\lfloor \cdot \rfloor$ is the floor function. Therefore, the total number of peaks in the oscillation region is $2n_{\text{peak}}(t) + 1$.

The spatial structure of the oscillations in the asymptotic state simplifies considerably as $t \to \infty$ as we show next. The key is to compute the limiting behavior of $m_n(t)$. Equation (6) yields simply $f(m) = O(1/t)$ as $t \to \infty$. Therefore, recalling again the behavior of $f(m)$ [cf. Fig. 1], we immediately see that $m_n(t) \to 1$ as $t \to \infty$. Since the limit $m \to 1$ of the solution (2) yields the classical (i.e., sech-shaped) solitons of Eq. (1) with zero background [41], this means that, perhaps surprisingly, *the long-time asymptotic behavior of modulationally unstable media is composed of an ensemble of classical solitons of the NLS equation* as opposed to the various breatherlike solutions with NZBCs, such as the Kuznetsov-Ma solitons [42,43], the Peregrine breather [44], the Akhmediev-Korneev breathers [36], and the more general Taijiri-Watanabe solitons [45]. We show below that this result is corroborated strongly by direct numerical simulations of Eq. (1).

The above results are also further strengthened by characterizing in detail the local structure of the asymptotic solution. To do so, one must compute the corrections to the leading-order behavior of $m_n(t)$. To this end, recall that the modulation parameters α_{re} and α_{im} do not depend on t explicitly but are instead just functions of m. Computing their asymptotic expansions with respect to m as $m \to 1$, which are given explicitly in the Appendix, Eq. (6) becomes $4q_o^2\sqrt{1-m} + O(1-m)^{3/2} = n/t$ as $m \to 1$. Solving this equation for $m = m_n(t)$ we obtain

$$m_n(t) = 1 - 1/\tau_n^2 + M_2(\tau_n)/\tau_n^4 + O\big[(\ln \tau_n)^4/\tau_n^6\big], \tag{9}$$

where we used the shorthand notation $\tau_n(t) = 4q_o^2 t/n$ and $M_2(\tau)$ is a quadratic polynomial in $\ln \tau$ (see the Appendix). Using Eq. (9) allows one to convert expansions as $m \to 1$ (which are computed in a straightforward way since all quantities are given explicitly in terms of m, see the Appendix) into expansions as $t \to \infty$. In particular, recalling Eq. (5), we have

$$x_n(t) = (n/q_o)\big[\ln \tau_n + 2 \ln 2 + 1 + X_2(\tau_n)/\tau_n^2 - X_4(\tau_n)/\tau_n^4\big] + O\big[(\ln \tau_n)^6/\tau_n^6\big], \quad t \to \infty, \tag{10}$$

where $X_2(\tau)$ and $X_4(\tau)$ are polynomials of degrees 2 and 4 in $\ln \tau$, respectively (see the Appendix). A comparison between the above expansion and a contour plot of the solution (2), shown in Fig. 2(left), demonstrates excellent agreement for all values of n and even for relatively small values of t. The velocity of the nth peak, given by $V_n = dx_n/dt$, is also easily computed from Eq. (10) and is

$$V_n(t) = 4q_o/\tau_n + O\big[(\ln \tau_n)^2/\tau_n^3\big], \qquad t \to \infty. \tag{11}$$

Note $V_n(t) \to 0$ as $t \to \infty$, i.e., all the peaks become asymptotically stationary as $t \to \infty$, but their position $x_n(t)$ diverges logarithmically in this limit.

The above results also allow us to compute the local shape of the modulated solution (2) in the neighborhood of one of the peaks. Using the above asymptotic expansions, one obtains an explicit expression for $|q_{\text{asymp}}(x,t)|$ near $x = x_n(t)$,

$$q_n(x,t) = A_n(t)\,\text{sech}\{2q_o[x - x_n(t)]\} + O(1/t^2), \tag{12}$$

as $t \to \infty$, where

$$A_n(t) = 2q_o\big[1 + (1 - \ln \tau_n)/\tau_n^2\big]. \tag{13}$$

A comparison between Eq. (12) for a few values of n and the modulated solution (2) is shown in Fig. 2, demonstrating excellent agreement. Note $A_n(t) \to 2q_o$ as $t \to \infty$. Therefore, *the long-time limit of the nonlinear stage of MI is characterized by an infinite ensemble of identical stationary sech-shaped solitons of the focusing NLS equation,* each with amplitude equal to twice that of the unstable background.

Robustness under perturbations. A natural question is whether the above behavior is robust. We can reformulate this question in terms of whether the results are stable under perturbations. The key dichotomy is whether the dynamics of the system under study is exactly governed by the NLS Eq. (1). If the answer is affirmative, the results of Ref. [14] establish rigorously the long-time asymptotics of the solution for any sufficiently localized ICs which do not generate a discrete spectrum from which the results of this Rapid Communication follow. On the other hand, if the NLS equation is only an approximate model of the actual behavior and the exact dynamics is governed by a perturbation of Eq. (1), the situation is different. This is because in many cases perturbed NLS equations give rise to chaotic behavior [33–35]. In that case, initially small differences between the exact solution of the NLS equation and that of the perturbed system will grow exponentially, and, as a result, the asymptotic state described in this Rapid Communication will not persist for all times. For example, this is the case when solving Eq. (1) numerically with periodic boundary conditions since in this case Eq. (1) is only an approximation of the dynamics due to truncation error. Indeed, such a scenario is characterized by catastrophic roundoff accumulation [33,34].

Nonetheless, even when integrating Eq. (1) numerically, an intermediate time range exists for which MI reaches the asymptotic state described in this Rapid Communication while the catastrophic roundoff has not yet taken hold. Recall that the growth rate of an unstable Fourier mode $\zeta \in [0,2\pi]$ is $\gamma(\zeta) = \zeta\sqrt{4q_o^2 - \zeta^2}$. Therefore $\gamma_{\max} = 2q_o^2$, which is achieved for $\zeta = \sqrt{2}q_o$. A simple calculation then shows that, working in double precision (i.e., with a machineilon of

10^{-16}), the time needed for roundoff error to become $O(1)$ is $\tau_{\text{roundoff}} = 16\ \ln(10)/\gamma_{\max} = 8\ \ln(10)/q_o^2$. One can expect that the asymptotic state described in this Rapid Communication will be destroyed by roundoff error after this time. On the other hand, we next show that the asymptotic state is robust up to $t = O(\tau_{\text{roundoff}})$.

To test the above results, we performed careful numerical simulations of Eq. (1) with several types of ICs on a nonzero background using an eighth-order split-step Fourier spectral method [46]. Owing to the scaling invariance of Eq. (1), we took $q_o = 1$ without loss of generality. For brevity, we only present the results for the following three kinds of ICs: Gaussian, sech-shaped, and boxlike, or, respectively,

$$q_{\text{Gaussian}}(x,0) = 1 + ie^{-x^2}\cos(\sqrt{2}x), \tag{14a}$$

$$q_{\text{sech}}(x,0) = 1 + i\ \text{sech}(10x), \tag{14b}$$

$$q_{\text{box}}(x,0) = \begin{cases} 1 + i\ \cos(\pi x), & |x| < 1, \\ 1, & \text{otherwise.} \end{cases} \tag{14c}$$

The numerical results as well as a comparison with the analytical predictions are shown in Fig. 3. Despite small individual variations among the three cases, the time evolution of the three ICs is remarkably similar and shows excellent agreement with the asymptotic predictions, including the boundary of the oscillation region, the location of the peaks, and the local shape of the solution near the peaks. This is true even for the IC (14c) which is discontinuous at $x = \pm 1$ and would therefore be expected to give rise to Gibbs-like dispersive oscillations [47,48]. (What this means is that the Gibbs-like dispersive oscillations produced by the discontinuity are small in amplitude and limited to short times and are quickly swamped by the developing growth of the oscillation structure produced by the modulational instability.) Similar results also were obtained with other kinds of localized ICs.

Discussion. We characterized the universal oscillation behavior of the nonlinear stage of MI under localized perturbations of the constant background. In particular, we gave explicit formulas for the number and locations of peaks, and we obtained asymptotic expressions for the shape of the solution near each peak in the long-time limit. We have also seen that, surprisingly, the long-time asymptotic behavior of MI is characterized by an ensemble of identical sech-shaped solitons of the NLS equation with zero background, each with amplitudes equal to twice that of the unstable background. Interestingly, this phenomenon is the opposite of that of the semiclassical limit of the focusing NLS equation with zero background in which the individual peaks have been shown to be accurately described by an ensemble of Peregrine breathers [49], which is a solution on a nonzero background.

Finally, we compared the theoretical results to numerical simulations with a variety of ICs. The numerical results therefore demonstrate not only the validity of the theoretical description, but also the universality and the robustness of the nonlinear stage of MI described in this Rapid Communication.

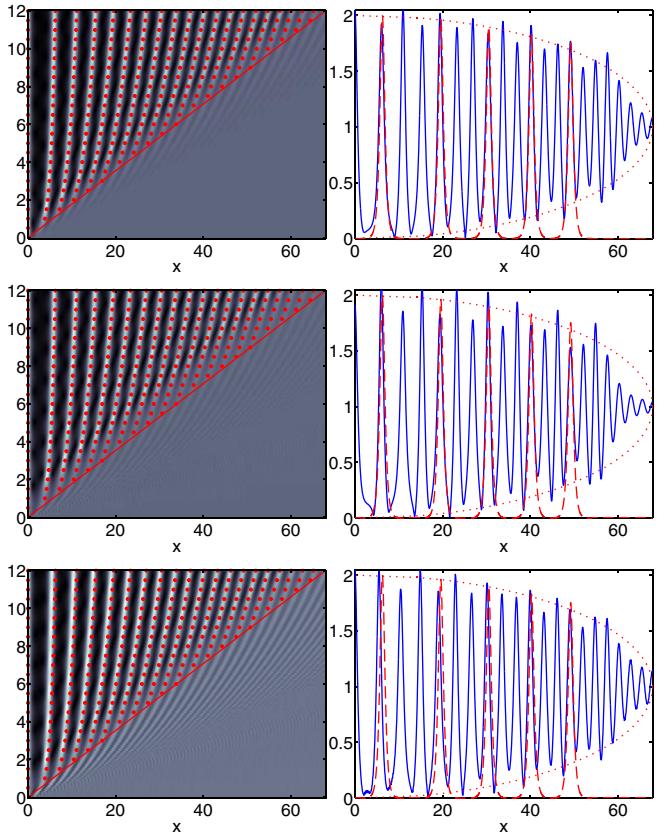

FIG. 3. Comparison between the theoretical prediction and the numerical solution $q(x,t)$ of Eq. (1) with three different ICs. Top row: Gaussian IC (14a); Center row: sech-shaped IC (14b); Bottom row: boxlike IC (14c). Left panels: density plot of $|q(x,t)|$ together with predicted boundary between the modulated region and the plane-wave region (red line) and location of peaks $x_n(t)$ (10) (red dots). Right panels: solution $|q(x,12)|$ (blue curve), selected five sech-like peaks (12) (dashed red curves), and predicted envelop (dotted red curves).

More in general, these results clearly demonstrate that the dynamics produced by the focusing NLS equation is different for systems with periodic BCs and systems on infinite spatial domains with NZBCs. In particular, we reiterate that the recurrence and chaotic dynamics present in the case of periodic BCs likely mean that no asymptotic state would emerge in that situation.

Since the NLS equation arises as a model in several physical settings and the results described in this Rapid Communication persist under perturbations, we believe that these phenomena should be observable experimentally. In particular, we hope that the present results will motivate experiments in deep water waves, optical fibers in the anomalous dispersion regime, and attracting Bose-Einstein condensates.

Acknowledgments. We thank M. Ablowitz, M. Onorato, and S. Trillo for many insightful discussions. This work was partially supported by the National Science Foundation under Grants No. DMS-1311847 and No. DMS-1614623.

APPENDIX

The solution of the system (3) yields

$$\xi(m) = \frac{4q_o\sqrt{m'}}{mE(m)} \times \frac{(1+m')E(m)K(m) + E^2(m) - 3m'K^2(m)}{\sqrt{E^2(m) - m'K^2(m)}}, \tag{A1a}$$

$$C(m) = (q_o/m)\sqrt{2 - m - 2m'K(m)/E(m)}. \tag{A1b}$$

with $m' = 1 - m$ for brevity. Recalling the asymptotic expansions of $K(m)$, $E(m)$, and $\mathrm{sn}(\cdot|m)$ as $m \to 0^+$ and as $m \to 1^-$ [38], one obtains

$$\alpha_{\mathrm{re}}(m) = \frac{\sqrt{2}}{2}q_o, \qquad \alpha_{\mathrm{im}}(m) = \frac{3}{8}q_o m, \qquad \xi(m) = 4\sqrt{2}q_o,$$

up to $O(m^2)$ terms as $m \to 0^+$ as well as

$$\alpha_{\mathrm{re}}(m) = 2q_o\sqrt{m'},$$
$$\alpha_{\mathrm{im}}(m) = q_o[1 + m'\ln m' + (2 - 4\ln 2)m'],$$
$$\xi(m) = 2q_o[2 + 4\ln 2 - \ln m']\sqrt{m'},$$

up to $O(m')^{3/2}$ terms as $m \to 1^-$. Next, to compute m as a function of t, we parametrize the elliptic parameter as

$$m = 1 - \Delta^2. \tag{A2}$$

Then by expanding the left-hand side of Eq. (6) as $\Delta \to 0$, one can solve recursively to compute all the terms in the expansion of Δ as a function of t. In this way we obtain

$$\Delta(t) = \frac{1}{\tau_n} - [2\ln^2\tau_n - 2(7 - 4\ln 2)\ln\tau_n + 15 + 4(\ln 2 - 7)\ln 2]\frac{1}{4\tau_n^3} + O\left[(\ln^4\tau_n)/\tau_n^5\right],$$

where we have used the shorthand notation $\tau_n(t) = 4q_o t^2/n$ as before. Substituting this expression into Eq. (A2), we then obtain Eq. (9), where

$$M_2(\tau) = \ln^2\tau + (4\ln 2 - 7)\ln\tau + 15/2 + 4\ln^2 2 - 14\ln 2.$$

Moreover, inserting Eq. (9) into Eq. (A1a), we obtain Eq. (10), where $X_2(\tau)$ and $X_4(\tau)$ are given by

$$X_2(\tau) = \tfrac{1}{4}[2\ln^2\tau + (8\ln 2 - 5)\ln\tau + 3 - 10\ln 2 + 8\ln^2 2],$$

$$X_4(\tau) = \tfrac{1}{128}[16\ln^4\tau + 32(4\ln 2 - 9)\ln^3\tau + 192(6 - 9\ln 2 + 2\ln^2 2)\ln^2\tau + 2(256\ln^3 2 - 1728\ln^2 2 + 2304\ln 2 - 997)\ln\tau + 1273 - 3908\ln 2 + 4608\ln^2 2 - 2304\ln^3 2 + 256\ln^4 2].$$

[1] V. E. Zakharov and L. A. Ostrovsky, Modulational instability: The beginning, Physica D **238**, 540 (2009).
[2] B. Kibler, J. Fatome, C. Finot, G. Millot, F. Dias, G. Genty, N. Akhmediev, and J. M. Dudley, The Peregrine soliton in nonlinear fibre optics, Nat. Phys. **6**, 790 (2010).
[3] D. R. Solli, C. Ropers, P. Koonath, and B. Jalali, Optical rogue waves, Nature (London) **450**, 1054 (2007).
[4] M. Onorato, A. R. Osborne, and M. Serio, Modulational Instability in Crossing Sea States: A Possible Mechanism for the Formation of Freak Waves, Phys. Rev. Lett. **96**, 014503 (2006).
[5] V. E. Zakharov, Turbulence in integrable systems, Stud. Appl. Math. **122**, 219 (2009).
[6] D. S. Agafontsev and V. E. Zakharov, Integrable turbulence and formation of rogue waves, Nonlinearity **28**, 2791 (2015).
[7] V. E. Zakharov and A. Gelash, Nonlinear Stage of Modulation Instability, Phys. Rev. Lett. **111**, 054101 (2013).
[8] B. Kibler, A. Chabchoub, A. Gelash, N. Akhmediev, and V. E. Zakharov, Superregular Breathers in Optics and Hydrodynamics: Omnipresent Modulation Instability Beyond Simple Periodicity, Phys. Rev. X **5**, 041026 (2015).
[9] S. Randoux, P. Walczak, M. Onorato, and P. Suret, Intermittency in Integrable Turbulence, Phys. Rev. Lett. **113**, 113902 (2014).
[10] M. Droques, B. Barviau, A. Kudlinski, M. Taki, A. Boucon, T. Sylvestre, and A. Mussot, Symmetry-breaking dynamics of the modulational instability spectrum, Opt. Lett. **36**, 1359 (2011).
[11] G. Biondini and G. Kovačič, Inverse scattering transform for the focusing nonlinear Schrödinger equation with nonzero boundary conditions, J. Math. Phys. **55**, 031506 (2014).
[12] G. Biondini and E. R. Fagerstrom, The integrable nature of modulational instability, SIAM J. Appl. Math. **75**, 136 (2015).
[13] G. Biondini and D. Mantzavinos, Universal Nature of the Nonlinear Stage of Modulational Instability, Phys. Rev. Lett. **116**, 043902 (2016).
[14] G. Biondini and D. Mantzavinos, Long-time asymptotics for the focusing nonlinear Schrödinger equation with nonzero boundary conditions at infinity and asymptotic stage of modulational instability, arXiv:1512.06095 [Commun. Pure Appl. Math. (to be published)].
[15] M. J. Ablowitz and H. Segur, *Solitons and the Inverse Scattering Transform* (SIAM, Philadelphia, 1981).
[16] G. P. Agrawal, *Nonlinear Fiber Optics* (Academic, New York, 2007).
[17] L. P. Pitaevskii and S. Stringari, *Bose-Einstein Condensation* (Clarendon, Oxford, 2003).
[18] N. I. Nikolov, T. Sørensen, O. Bang, and A. Bjarklev, Improving efficiency of supercontinuum generation in photonic crystal fibers by direct degenerate four-wave mixing, J. Opt. Soc. Am. B **20**, 2329 (2003).
[19] M. H. Frosz, T. Sørensen, and O. Bang, Nanoengineering of photonic crystal fibers for supercontinuum spectral shaping, J. Opt. Soc. Am. B **23**, 1692 (2006).

[20] S. T. Sørensen, C. Larsen, U. Møller, P. M. Moselund, C. L. Thomsen, and O. Bang, Influence of pump power and modulation instability gain spectrum on seeded supercontinuum and rogue wave generation, J. Opt. Soc. Am. B **29**, 2875 (2012).

[21] J. R. Ott, M. Heuck, C. Agger, P. D. Rasmussen, and O. Bang, Label-free and selective nonlinear fiber-optical biosensing, Opt. Express **16**, 20834 (2008).

[22] C. Markos and O. Bang, Nonlinear label-free biosensing with high sensitivity using As_2S_3 chalcogenide tapered fiber, J. Lightwave Technol. **33**, 2892 (2015).

[23] M. H. Frosz, A. Stefani, and O. Bang, Highly sensitive and simple method for refractive index sensing of liquids in microstructured optical fibers using four-wave mixing, Opt. Express **19**, 10471 (2011).

[24] B. Gu, W. Yuan, M. H. Frosz, A. P. Zhang, S. He, and O. Bang, Nonlinear fiber-optic strain sensor based on four-wave mixing in microstructured optical fiber, Opt. Lett. **37**, 794 (2012).

[25] H. C. Yuen and W. E. Ferguson, Relationship between Benjamin-Feir instability and recurrence in the nonlinear Schrödinger equation, Phys. Fluids **21**, 1275 (1978).

[26] E. Fermi, J. Pasta, and S. Ulam, in *Collected Papers of Enrico Fermi*, edited by E. Segré (The University of Chicago, Chicago, 1965), Vol. 2.

[27] B. M. Lake, H. C. Yuen, H. Rungaldier, and W. E. Ferguson, Nonlinear deep-water waves: Theory and experiment. Part 2. Evolution of a continuous wave train J. Fluid Mech. **83**, 49 (1977).

[28] H. C. Yuen, B. M. Lake, and W. E. Ferguson, *The Significance of Nonlinearity in the Natural Science* (Plenum, New York, 1977).

[29] N. N. Akhmediev, Nonlinear physics: Déjà vu in optics, Nature (London) **413**, 267 (2001).

[30] G. Van Simaeys, P. Emplit, and M. Haelterman, Experimental Demonstration of the Fermi-Pasta-Ulam Recurrence in a Modulationally Unstable Optical Wave, Phys. Rev. Lett. **87**, 033902 (2001).

[31] B. Zhao, D. Y. Tang, and H. Y. Tam, Experimental observation of FPU recurrence in a fiber ring laser, Opt. Express **11**, 3304 (2003).

[32] M. Erkintalo, K. Hammani, B. Kibler, C. Finot, N. N. Akhmediev, J. M. Dudley, and G. Genty, Higher-Order Modulation Instability in Nonlinear Fiber Optics, Phys. Rev. Lett. **107**, 253901 (2011).

[33] M. J. Ablowitz and B. M. Herbst, On homoclinic structure and numerically induced chaos for the nonlinear Schrödinger equation, SIAM J. Appl. Math. **50**, 339 (1990).

[34] M. J. Ablowitz, C. M. Schober, and B. M. Herbst, Numerical Chaos, Roundoff Errors and Homoclinic Manifolds, Phys. Rev. Lett. **71**, 2683 (1993).

[35] M. J. Ablowitz, J. Hammack, D. Henderson, and C. M. Schober, Modulated Periodic Stokes Waves in Deep Water, Phys. Rev. Lett. **84**, 887 (2000).

[36] N. N. Akhmediev and V. I. Korneev, Modulational instability and periodic solutions of the nonlinear Schrödinger equation, Theor. Math. Phys. **69**, 1089 (1987).

[37] S. Trillo and S. Wabnitz, Dynamics of the nonlinear modulational instability in optical fibers, Opt. Lett. **16**, 986 (1991).

[38] F. W. Olver, D. W. Lozier, R. F. Boisvert, and C. W. Clark, *NIST Handbook of Mathematical Functions* (Cambridge University Press, New York, 2010).

[39] A. M. Kamchatnov, *Nonlinear Periodic Waves and Their Modulations: An Introductory Course* (World Scientific, Singapore, 2000).

[40] G. A. El, A. V. Gurevich, V. V. Khodorovskiĭ, and A. L. Krylov, Modulational instability and formation of a nonlinear oscillatory structure in a focusing medium, Phys. Lett. A **177**, 357 (1993).

[41] V. E. Zakharov and A. B. Shabat, Exact theory of two-dimensional self-focusing and one-dimensional self-modulation of waves in nonlinear media, Sov. Phys. JETP **34**, 62 (1972).

[42] E. A. Kuznetsov, Solitons in a parametrically unstable plasma, Sov. Phys. Dokl. **22**, 507 (1977).

[43] Y.-C. Ma, The perturbed plane-wave solutions of the cubic Schrödinger equation, Stud. Appl. Math. **60**, 43 (1979).

[44] D. H. Peregrine, Water waves, nonlinear Schrödinger equations and their solutions, Austral. Math. Soc. Ser. B **25**, 16 (1983).

[45] M. Tajiri and Y. Watanabe, Breather solutions to the focusing nonlinear Schrödinger equation, Phys. Rev. E **57**, 3510 (1998).

[46] H. Yoshida, Construction of higher order symplectic integrators, Phys. Lett. A **150**, 262 (1990).

[47] J. C. DiFranco and K. T.-R. McLaughlin, A nonlinear Gibbs-type phenomenon for the defocusing nonlinear Schrödinger equation, Int. Math. Res. Papers **2005**, 403.

[48] G. Biondini and T. Trogdon, Gibbs phenomenon for dispersive PDEs, arXiv:1411.6142.

[49] M. Bertola and A. Tovbis, Universality for the focusing nonlinear Schrödinger equation at the gradient catastrophe point: Rational breathers and poles of the tritronquée solution to Painlevé I, Commun. Pure Appl. Math. **66**, 678 (2013).